Hybrid lattice Boltzmann model for atmospheric flows under anelastic approximation

Y. Feng, J. Miranda-Fuentes, Jérôme Jacob, Pierre Sagaut

Hybrid lattice Boltzmann model for atmospheric flows under anelastic approximation

Y. Feng (封永亮),[a] J. Miranda-Fuentes, J. Jacob, and P. Sagaut

AFFILIATIONS

Aix Marseille Univ, CNRS, Centrale Marseille, M2P2 UMR 7340, 13451 Marseille, France

ABSTRACT

Lattice Boltzmann (LB) method for atmospheric dynamics is developed by considering the characteristics of the anelastic approximation. After introducing reference base state values in atmospheric flows, an LB model, with an external force term, has been constructed in anelastic framework. In the proposed anelastic LB model, mass and momentum conservation equations are solved by the LB method with a regularization procedure, and temperature field or scalar transport is simulated by finite volume method. The derived macroscopic governing equations from the anelastic model are analyzed and discussed in Chapman–Enskog asymptotic expansion. The anelastic LB model is assessed considering three benchmarks including a non-hydrostatic atmospheric inviscid convection, two-dimensional density currents, and inertia-gravity waves in stably stratified atmospheric layer. The validations demonstrate that the anelastic extension of the LB method can simulate atmospheric flows effectively and accurately. Besides, the proposed model offers a unified framework for both Boussinesq approximation and anelastic approximation, which is largely free of characteristic depth of atmospheric flows.

I. INTRODUCTION

Atmospheric dynamics is composed of motions occurring on a wide range of temporal and spatial scales, including propagating waves of various types, buoyancy-driven convection, thermal stratification, etc. To better understand atmospheric flows and related environment science, numerical simulation is a good complement to field measurements and wind tunnel experiments.[1–3] Modeling these hydro-thermo-dynamical phenomena requires numerical methods for solving a system of partial differential equations originating from Navier–Stokes equations. The scales of motion in the atmospheric flows can be all captured by the fully compressible Navier–Stokes equations, which are the most complete approaches involving all physical mechanisms. However, as acoustic modes do not play an important role in atmospheric dynamics, it is theoretically appealing and also numerically advantageous to remove the sound waves entirely from the governing equations.[4]

Relative to the full compressible Navier–Stokes equations, the anelastic model filter acoustic waves while maintaining advection-diffusion of momentum and supporting internal gravity waves.[5–7] The anelastic approximation accounts for large vertical variations of pressure and density but disregards the time derivative of the density in the continuity equation, which is widely employed in atmospheric deep convection simulations. In conventional computational fluid dynamics framework, the fractional-step method is widely used in solving the anelastic equations.[8] Due to advantages of the lattice Boltzmann method (LBM) for massively parallel computing as well as its high fidelity and low dispersion, there are significant research efforts devoted to extending LBM to large-scale urban flows and shallow atmospheric boundary layer flows.[9–12]

The LBM is originally a weakly compressible flows solver, which has been developed to an efficient method for complex flows.[13,14] The applications of LBM cover, among others, aerodynamic studies on full-scale vehicles, turbulent flows in urban areas,[15] aerodynamic predictions on airfoils.[16] Furthermore, the LBM has also been extended to complex multi-physics phenomena through coupling the additional conservation laws.[17–20]

The LB models for atmospheric dynamics could be straightforwardly developed by targeting to compressible Navier–Stokes equation at low Mach limit, considering the density stratification and weakly compressible feature of atmospheric flows. A set of thermal LB models was proposed for simulation of low Mach and high Mach number flows.[21–24] However, the time step or Courant–Friedrichs–Lewy (CFL) number is narrowed in the thermal LB models when it targets to solve the fully coupled compressible flow system. The compressible LB

models use the acoustic time step required for numerical stability. This is impractical from the perspective of weather and climate. Therefore, a soundproof LB model could be constructed from incompressible LB models in which the compressibility effect is effectively reduced. Zou *et al.*[25] made the first attempt to construct an incompressible LB model for steady flows. He and Luo[26] developed another general incompressible LB model, which approximately recovers artificial compressible version of the incompressible Navier–Stokes equations. Subsequently, Guo *et al.*[27] developed a pressure-based incompressible LB model to recover the incompressible Navier–Stokes equations for both unsteady and steady flows, which achieved an $O(Ma^2)$ accuracy. However, most of these incompressible LB models were developed for flows with uniform density, which is only available under Bousssinesq approximation in shallow atmosphere where the density variations are often small compared with the mean fluid density. An important extension of LB method to shallow water equation with nonhydrodynamic modes was proposed and analyzed by Dellar.[28] Several LB models for simulation of shallow water were developed,[29–31] but the shallow water LB models mainly focus on hydraulics behavior. Conclusively, a LBM with anelastic approximation is required for modeling atmospheric flows with deep convection.

Due to the feature of large spatial scales and strong convection, the numerical stability of collision model is among the key issues faced when developing a LB model for atmospheric flows. The most commonly used lattice Boltzmann collision model is the single-time relaxation process, which is the so-called lattice Bhatnagar–Gross–Krook (LBGK) model.[32] In order to overcome the insufficient stability observed in the LBGK model, several improved collision models with enhanced stability have been proposed. The multiple relaxation time (MRT) model was proposed by Lallemand and Luo,[33] in which collision process is modeled in the moment space rather than in discrete velocities space in the BGK model. The entropic lattice Boltzmann (ELB) model was developed by introducing a stabilizing process via Boltzmann's H theorem.[34] Besides, the cascaded LB,[35] central moment LB,[36,37] and cumulant LB[38] models were proposed to improve the stability and accuracy using central moment or cumulant. Recently, both basic and improved regularized LBGK (RLBGK) model is developed to higher-order lattices both for high Reynolds number flows and for high Mach number flows.[39–41] In RLBGK method, a pre-collision operator is introduced to improve convergence properties at a very moderate computational overhead. These models were shown to provide significant improvements over the LBGK method in many high Reynolds number flows. Moreover, the regularized LBGK model appears to offer a simple and parameter-free option to save significant computational costs over the LBGK model.

Hybrid LBM has been widely adopted in thermal flows and scalar transport process. A hybrid thermal LB model has been proposed by Lallemand *et al.*,[17] where a finite difference algorithm was adopted to solve energy-conservation equation. A hybrid finite difference thermal lattice model has been widely studied in nearly incompressible convective flows.[42] Besides, a hybrid finite difference thermal model using two-dimensional multiple relaxation time collision model has been presented for low Mach number compressible flows.[43] As reported in studies of Li *et al.*,[44] the hybrid finite difference thermal model can simply avoid a spurious source term in thermal LB models with force terms. Besides, the computational efficiency of hybrid approach was gained in simulation of thermal flows.[45]

To this end, we aim at developing a LB model for anelastic approximation, which can effectively extend the application from shallow convection under Boussinesq approximation to atmospheric flows with arbitrary depth. It provides an alternative method for the numerical simulation of both deep and shallow convection in atmospheric flows. Indeed, an extension of LBM for anelastic approximation could extend the application of LBM to shallow and deep convection in a simple and efficient way. The rest of this article is organized as follows. In Sec. II, the mathematical approximations done on compressible Navier–Stokes equations and anelastic approximation are introduced. In Sec. III, the hybrid LB model with anelastic approximation is proposed, which is based on standard equilibrium distribution with an external force term corresponding to the anelastic approximation. In Sec. IV, validation of the proposed model is conducted by simulating benchmark solutions including a non-hydrostatic atmospheric inviscid convection case, two-dimensional density currents, and inertia-gravity wave in stable atmospheric layer. Finally, a conclusion section is given.

II. PHYSICAL GOVERNING EQUATIONS

Although the motion of atmospheric dynamics can be straightforwardly described by compressible Navier–Stokes (NS) equations, the scale-dependent models for atmospheric flows are theoretically appealing and also numerically advantageous to remove the sound waves from the NS equations. The anelastic approximation is motivated by atmospheric flows for which the effects of stratification are important.[5,46] Acoustic waves are thereby filtered – hence, the term anelastic, meaning acoustic-elastic energy is not allowed. In this section, the basic equations of anelastic approximation are recalled from the classical compressible NS equation. Then, a variant form of the anelastic equations is rewritten to allow the possibility that the equations can be solved by the LBM.

A. Reminders about compressible Navier–Stokes equation

The governing equations by using entropy variable s govern the motion for a compressible atmosphere without rotation and friction for brevity under a uniform gravity $g_\alpha = (0, 0, g_z)$ are[47,48]

$$\frac{\partial \rho}{\partial t} + \frac{\partial}{\partial x_\alpha}(\rho u_\alpha) = 0, \tag{1a}$$

$$\rho \frac{\partial u_\alpha}{\partial t} + \rho u_\beta \frac{\partial u_\alpha}{\partial x_\beta} = -\frac{\partial p}{\partial x_\alpha} - \rho g_\alpha, \tag{1b}$$

$$\rho \frac{\partial s}{\partial t} + \rho u_\alpha \frac{\partial s}{\partial x_\alpha} = \frac{Q_r}{T}, \tag{1c}$$

where the subscript α represents Cartesian coordinates (x, y, z). ρ, $u_\alpha = (u, v, w)$, and s is the density, velocity, and entropy, respectively. The pressure $p = \rho RT$ satisfies thermodynamic equation of state with gas constant R and temperature T. Q_r is heat rate per unit volume. Potential temperature θ is a more dynamically important quantity than the actual temperature T, which can be linked with entropy s and temperature as[47]

$$s = C_p \ln \frac{\theta}{\theta_{00}}, \quad s = C_v \ln \frac{T}{\rho^{\gamma-1}}, \tag{2}$$

where C_p is specific heat capacity at constant pressure, $\gamma = C_p/(C_p - R)$ is specific heat ratio, and θ_{00} is a nominal reference value for

the potential temperature. Thus, the energy equation (1c) can be rewritten as[49]

$$\rho\frac{\partial\theta}{\partial t}+\rho u_\alpha\frac{\partial\theta}{\partial x_\alpha}=\frac{\theta}{C_pT}Q_r. \tag{3}$$

A relation between the potential temperature θ and actual temperature T can be derived from Eq. (2) as[49]

$$T=\pi\theta,\quad \pi=\left(\frac{p}{p_{00}}\right)^{R/C_p},\quad \theta_{00}=\left(\frac{p_{00}}{R}\right)^{R/C_p}, \tag{4}$$

where $p_{00}=1000$ mb is constant reference pressure commonly used in the atmospheric flows.

B. Anelastic approximation

The state variables are described as small fluctuations ($'$ superscript) from corresponding vertical reference base state profiles ($_s$ subscript), which are the functions of altitude only. Here, ρ_s and p_s are the base state density and pressure, respectively. θ_s is base state potential temperature, which servers as a basis for the potential temperature splitting $\theta=\theta_s+\theta'$. Considering scale analysis in[5]

$$\frac{\mathrm{D}p_s}{\mathrm{D}z}=-\rho_s g, \tag{5}$$

and using hydrostatic relation about base state variables, one can rewrite the continuity, momentum equations, and energy equation as follows:[5]

$$\frac{\partial\rho_s u_\alpha}{\partial x_\alpha}=0, \tag{6a}$$

$$\rho_s\frac{\partial u_\alpha}{\partial t}+\rho_s u_\beta\frac{\partial u_\alpha}{\partial x_\beta}=-\frac{\partial p'}{\partial x_\alpha}-\rho' g_\alpha, \tag{6b}$$

$$\rho_s\frac{\partial\theta}{\partial t}+\rho_s u_\alpha\frac{\partial\theta}{\partial x_\alpha}=\frac{Q_r}{C_p}, \tag{6c}$$

where ρ', θ, and p' are perturbation density, potential temperature, and pressure, respectively. The thermodynamic relation between the fluctuations of potential temperature, pressure, and density under the anelastic approximation is[5]

$$\frac{\rho'}{\rho_s}=\frac{p'}{\rho_s g H_\rho}-\frac{\theta'}{\theta_s}, \tag{7}$$

where scale of heights H_ρ is defined as

$$\frac{1}{H_\rho}=\frac{1}{\rho_s}\frac{\mathrm{D}\rho_s}{\mathrm{D}z}. \tag{8}$$

It is important to emphasize that the diagnostic relation Eq. (7) is the key closure assumption for anelastic theory. By using Eq. (7), the right-hand side of Eq. (6b) can be written as

$$-\frac{\partial p'}{\partial x_\alpha}-\rho' g_\alpha=\rho_s\left[-\frac{\partial(p'/\rho_s)}{\partial x_\alpha}+\frac{\theta'}{\theta_s}g\right]. \tag{9}$$

Using the thermodynamic relation between the fluctuations and height scale H_ρ, Eq. (9) and supplying the viscous and diffusion terms, the anelastic viscous equations can be rewritten as

$$\frac{\partial u_\alpha}{\partial x_\alpha}=-wH_\rho^{-1}, \tag{10a}$$

$$\frac{\partial u_\alpha}{\partial t}+u_\beta\frac{\partial u_\alpha}{\partial x_\beta}=-\frac{\partial p''}{\partial x_\alpha}+\nu\frac{\partial^2 u_\alpha}{\partial x_\beta^2}+\frac{\theta'}{\theta_s}g, \tag{10b}$$

$$\frac{\partial\theta}{\partial t}+u_\alpha\frac{\partial\theta}{\partial x_\alpha}=\frac{1}{\rho_s}\frac{\partial}{\partial x_\alpha}\left(D_\theta\frac{\partial\theta}{\partial x_\alpha}\right)+\frac{Q_r}{C_p\rho_s}, \tag{10c}$$

where $p''=p'/\rho_s$. Equations (10a)–(10c) are macroscopic equations, which will be used to construct an anelastic LB model in this study. If the vertical scale of motion is small compared with the depth of an adiabatic atmosphere,

$$H_\rho\approx\infty,\quad \rho_s\approx\rho_0. \tag{11}$$

The anelastic equations reduce to the Boussinesq equations for shallow convection,[50,51]

$$\frac{\partial u_\alpha}{\partial x_\alpha}=0, \tag{12a}$$

$$\frac{\partial u_\alpha}{\partial t}+u_\beta\frac{\partial u_\alpha}{\partial x_\beta}=-\frac{\partial p''}{\partial x_\alpha}+\nu\frac{\partial^2 u_\alpha}{\partial x_\beta^2}+\frac{\theta'}{\theta_0}g_\alpha, \tag{12b}$$

$$\frac{\partial\theta}{\partial t}+u_\alpha\frac{\partial\theta}{\partial x_\alpha}=\frac{1}{\rho_0}\frac{\partial}{\partial x_\alpha}\left(D_\theta\frac{\partial\theta}{\partial x_\alpha}\right)+\frac{Q_r}{C_p\rho_0}. \tag{12c}$$

It removes the limitation of Boussinesq approximation, especially on vertical direction in which the characteristic vertical displacement of an air parcel is comparable with the density scale height and the horizontal variations of the thermodynamic variables are small.[52]

III. LATTICE BOLTZMANN METHOD FOR ANELASTIC APPROXIMATION

A. Classical nearly incompressible LB model

LBMs aim at solving the lattice Boltzmann equation through space, time, *and velocity* discretization.[53,54] Space and time are classically discretized on a Cartesian grid, whereas speeds are discretized on the so-called DnQm lattice (n dimensions and m discrete velocities $c_{i,\alpha}$, i being index of discrete velocities.).

The flow problem is then solved for $f_i(x_\alpha,t)$, the density distribution of particles with velocity $c_{i,\alpha}$ at (x_α,t), which can be obtained at time $t+\delta_t$ through the so-called LBGK collision model[53]

$$f_i(x_\alpha+c_{i,\alpha}\delta_t,t+\delta_t)=f_i(x_\alpha,t)-\frac{1}{\bar{\tau}}\left[f_i(x_\alpha,t)-f_i^{eq}(x_\alpha,t)\right]+\left(1-\frac{1}{2\bar{\tau}}\right)\delta_t F_i(x_\alpha,t), \tag{13}$$

a succession of a streaming and a collision step[26,53] which is equivalent to a Strang-splitting-based time integration method.[55] The nondimensional collision time $\bar{\tau}$ is related to the kinematic viscosity ν through $\nu=c_s^2(\bar{\tau}-\frac{1}{2})\delta_t$, and c_s is the lattice sound speed, inherent of the lattice DnQm choice.[56]

The incompressible LB models have been proposed by He *et al.*[26] and Guo *et al.*[27] In this study, the equilibrium distribution of the basic incompressible LB model is expanded to the third order to further reduce Galilean invariant error, which is expressed as follows:

$$f_i^{eq} = \rho\lambda_i + w_i\left[\frac{c_{i\alpha}}{c_s^2}u_\alpha + \frac{\mathscr{H}^{(2)}_{i,\alpha\beta}}{2c_s^4}u_\alpha u_\beta + \frac{\mathscr{H}^{(3)}_{i,\alpha\beta\gamma}}{6c_s^6}u_\alpha u_\beta u_\gamma\right], \tag{14}$$

where $\lambda_0 = w_0 - 1$ for stationary discrete velocity, $\lambda_i = w_i$ for the rest of discrete velocities. $\mathscr{H}^{(3)}_{i,\alpha\beta\gamma} = c_{i,\alpha}c_{i,\beta}c_{i,\gamma} - c_s^2[c_i\delta]_{\alpha\beta\gamma}$ where $[c_i\delta]_{\alpha\beta\gamma}$ $= c_{i,\alpha}\delta_{\beta\gamma} + c_{i,\beta}\delta_{\alpha\gamma} + c_{i,\gamma}\delta_{\alpha\beta}$. The moments of the equilibrium distribution function are summarized as follows:

$$\sum_i f_i^{eq} = 0, \tag{15a}$$

$$\sum_i f_i^{eq}c_{i,\alpha} = u_\alpha, \tag{15b}$$

$$\sum_i f_i^{eq}c_{i,\alpha}c_{i,\beta} = \rho c_s^2\delta_{\alpha\beta} + u_\alpha u_\beta, \tag{15c}$$

$$\sum_i f_i^{eq}c_{i,\alpha}c_{i,\beta}c_{i,\gamma} = c_s^2[u\delta_{\alpha\beta\gamma}] + u_\alpha u_\beta u_\gamma + \Phi_{\alpha\beta\gamma}, \tag{15d}$$

where $[u\delta_{\alpha\beta\gamma}] = u_\alpha\delta_{\beta\gamma} + u_\beta\delta_{\gamma\alpha} + u_\gamma\delta_{\beta\alpha}$. The symmetry-breaking error $\Phi_{\alpha\beta\gamma}$ is due to the topology of the nearest-neighbor lattices (D2Q9, D3Q19, and D3Q27), $\Phi_{\alpha\beta\gamma} = 0$ except for $\Phi_{\alpha\alpha\alpha} = -\rho u_\alpha^3$. The deviation induced by $\Phi_{\alpha\beta\gamma}$ can be neglected in atmospheric flows at low Mach number.

The solutions of the lattice Boltzmann equation approximate the macroscopic equations

$$\frac{\partial u_\alpha}{\partial x_\alpha} = 0, \tag{16a}$$

$$\frac{\partial u_\alpha}{\partial t} + u_\beta\frac{\partial u_\alpha}{\partial x_\beta} = -\frac{\partial p}{\partial x_\alpha} + \nu\frac{\partial^2 u_\alpha}{\partial x_\beta^2} + \mathscr{O}(Ma^2). \tag{16b}$$

It is well known that Eq. (16) by the incompressible LB model is only applicable for flows with a uniform density field.

B. Anelastic lattice Boltzmann model

An anelastic model within the framework of LBMs for atmospheric flows with a height-dependent density is developed in this section. In anelastic approximation, acoustic waves are filtered and pressure is expanded into the sum of a vertical reference pressure and pressure fluctuations. The small pressure fluctuations are decoupled from corresponding vertical reference density and pressure.

In the present study, an approach using external force terms is proposed to develop an anelastic LB model based on standard LB model (e.g., D2Q9, D3Q19). This is done by introducing an external force term ψ_i into generic force F_i and its moments are expressed as

$$\sum_i \psi_i = \Psi_0, \tag{17a}$$

$$\sum_i \psi_i c_{i,\alpha} = \Psi_\alpha, \tag{17b}$$

$$\sum_i \psi_i c_{i,\alpha}c_{i,\beta} = \Psi_{\alpha\beta}. \tag{17c}$$

It is worth noting that the moments of force term ψ_i, Ψ_0, Ψ_α and $\Psi_{\alpha\beta}$ are under-determined. The exact expressions of them are determined by considering that the proposed LB model recovers anelastic Eq. (10).

The same evolution equation and equilibrium distribution functions as with a standard LB model are adopted in the model.

To derive macroscopic equations under anelastic approximation with external force terms, the density distribution function f_i is expanded around the f_i^{eq} distributions as follows: To derive macroscopic equations, the density distribution function f_i is expanded around the f_i^{eq} distributions as follows:

$$f_i = f_i^{(0)} + \varepsilon f_i^{(1)} + \varepsilon^2 f_i^{(2)} + \cdots, \tag{18}$$

with

$$\sum_i f_i^{(n)} = 0, \quad \sum_i c_{i\alpha}f_i^{(n)} = 0, \ n > 0. \tag{19}$$

By matching the scales of ε^1, ε^2, we have

$$\varepsilon^1 : \left(\frac{\partial}{\partial t_1} + c_{i\alpha}\frac{\partial}{\partial x_{1\alpha}}\right)f_i^{eq} + \frac{f_i^{(1)}}{\tau} = \psi_i^{(0)}, \tag{20}$$

$$\varepsilon^2 : \frac{\partial f_i^{eq}}{\partial t_2} + \left(\frac{\partial}{\partial t_1} + c_{i\alpha}\frac{\partial}{\partial x_{1\alpha}}\right)f_i^{(1)} + \frac{f_i^{(2)}}{\tau} = 0. \tag{21}$$

Considering that the equilibrium density distribution function satisfies the velocity moment condition, one can sum Eqs. (20) and (21) in the velocity phase space. The t_1 and t_2 order of the continuity equation and momentum equation can be derived as

$$\frac{\partial u_\alpha}{\partial x_{1\alpha}} = \Psi_0, \tag{22}$$

$$\frac{\partial u_\alpha}{\partial t_1} + \frac{\partial}{\partial x_{1\beta}}(u_\alpha u_\beta + \rho c_s^2\delta_{\alpha\beta}) = \Psi_\alpha, \tag{23}$$

$$\frac{\partial u_\alpha}{\partial t_2} + \frac{\partial}{\partial x_{1\beta}}\left(\sum_i c_{i\alpha}c_{i\beta}f_i^{(1)}\right) = 0. \tag{24}$$

Rewriting $f_i^{(1)}$ in Eq. (24) with Eqs. (22) and (23), one obtains

$$\begin{aligned}\Pi_{\alpha\beta} &= \sum_i c_{i\alpha}c_{i\beta}f_i^{(1)} \\ &= -\tau\sum_i c_{i\alpha}c_{i\beta}\left[\left(\frac{\partial}{\partial t_1} + c_{i\alpha}\frac{\partial}{\partial x_{1\alpha}}\right)f_i^{eq} - \psi_i^{(0)}\right] \\ &= -\tau\left[c_s^2\left(\frac{\partial u_\beta}{\partial x_\alpha} + \frac{\partial u_\alpha}{\partial x_\beta}\right) + (c_s^2\delta_{\alpha\beta} - u_\alpha u_\beta)\Psi_0\right. \\ &\quad \left. + u_\alpha\Psi_\beta + u_\beta\Psi_\alpha - \Psi_{\alpha\beta} + \mathscr{O}(Ma^3)\right].\end{aligned} \tag{25}$$

Using Eqs. (22) and (23), the above equation can be further approximated as follows:

$$\frac{\partial\Pi_{\alpha\beta}}{\partial x_\beta} = \nu\frac{\partial^2 u_\alpha}{\partial x_\beta^2} + \nu\frac{\partial}{\partial x_\alpha}\frac{\partial u_\beta}{\partial x_\beta} + \mathscr{O}\left(\frac{Ma^3}{Re}\right), \tag{26}$$

where Ma and Re number is, respectively, defined as $Ma = u_\alpha/c_s$ and $Re = u_\alpha H_\rho/\nu$. Due to $\partial u_\beta/\partial x_\beta = \Psi_0 = w/H_\rho \neq 0$, a compensation term $\nu\partial(w/H_\rho)/\partial x_\alpha$ is added in Ψ_α. The second-order force terms $\Psi_{\alpha\beta}$ is given as

$$\Psi_{\alpha\beta} = (c_s^2\delta_{\alpha\beta} - u_\alpha u_\beta)\Psi_0 + u_\alpha\Psi_\beta + u_\beta\Psi_\alpha. \tag{27}$$

The following viscous term in recovered macroscopic equations can be derived as

$$\Pi_{\alpha\beta} = \nu \frac{\partial u_\alpha}{\partial x_\beta}, \quad \frac{\partial \Pi_{\alpha\beta}}{\partial x_\beta} = \nu \frac{\partial^2 u_\alpha}{\partial x_\beta^2} + \mathcal{O}\left(\frac{Ma^3}{Re}\right). \tag{28}$$

The term $u_\alpha \Psi_0 = -u_\alpha w/H_\rho$ is of order of $\mathcal{O}(Ma^2 H_\rho^{-1})$, the convective term is given as

$$\frac{\partial}{\partial x_\beta}(u_\alpha u_\beta) = u_\beta \frac{\partial u_\alpha}{\partial x_\beta} + u_\alpha \frac{\partial u_\beta}{\partial x_\beta} = u_\beta \frac{\partial u_\alpha}{\partial x_\beta} + \mathcal{O}\left(\frac{Ma^2}{H_\rho}\right). \tag{29}$$

By applying the above results, the following anelastic equations are recovered by the proposed LB model,

$$\frac{\partial u_\alpha}{\partial x_\alpha} = -wH_\rho^{-1}, \tag{30a}$$

$$\frac{\partial u_\alpha}{\partial t} + u_\beta \frac{\partial u_\alpha}{\partial x_\beta} = -\frac{\partial p''}{\partial x_\alpha} + \nu \frac{\partial^2 u_\alpha}{\partial x_\beta^2} + \frac{\theta'}{\theta_s} g + \mathcal{O}\left(\frac{Ma^3}{Re} + \frac{Ma^2}{H_\rho}\right), \tag{30b}$$

where $\Psi_\alpha = g\theta'/\theta_s - \nu\partial(w/H_\rho)/\partial x_\alpha$ and $p'' = (\rho - \rho_0)c_s^2$ are applied. Finally, the solutions of the proposed lattice Boltzmann equation approximate the macroscopic anelastic equations for atmospheric flows.

C. Recursive regularized LB model with forcing term

The regularization procedures were proposed for improve stability of LBMs.[57] They play the role of a filter on undesirable ghost moments of the numerical scheme. The accuracy and stability of regularized BGK model were well analyzed in both inviscid acoustic problems[58] and turbulent flows.[59] Practically, a regularized distribution function is introduced through recomputing the non-equilibrium parts prior to the collision step. The lattice Boltzmann BGK equation with recursive regularization is expressed as

$$f_i(x_\alpha + c_{i\alpha}\delta_t, t + \delta_t) = f_i^{eq}(x_\alpha, t) + \left(1 - \frac{1}{\bar{\tau}}\right)\mathscr{R}(f_i^{neq}) + \frac{\delta_t}{2}\psi_i(x_\alpha, t), \tag{31}$$

where the off-equilibrium distribution function is expressed as

$$f_i^{neq} = f_i(x_\alpha, t) - f_i^{eq}(x_\alpha, t) + \frac{\delta_t}{2}\psi_i(x_\alpha, t). \tag{32}$$

$\mathscr{R}(f_i^{neq})$ is recursive regularization operator

$$\mathscr{R}(f_i^{neq}) = w_i \left[\frac{\mathscr{H}_{i\alpha\beta}}{2c_s^4}\mathscr{A}_{\alpha\beta}^{(1)} + \frac{\mathscr{H}_{i\alpha\beta\gamma}}{6c_s^6}\mathscr{A}_{\alpha\beta\gamma}^{(1)}\right], \tag{33}$$

where $\mathscr{A}_{\alpha\beta}^{(1)} = \sum_i c_{i\alpha}c_{i\beta}f_i^{neq}$ is the second-order off-equilibrium moment and the third-order off-equilibrium moment is recursively computed by using $\mathscr{A}_{\alpha\beta\gamma}^{(1)} = u_\alpha \mathscr{A}_{\beta\gamma}^{(1)} + u_\beta \mathscr{A}_{\gamma\alpha}^{(1)} + u_\gamma \mathscr{A}_{\alpha\beta}^{(1)}$. For the proposed anelastic LB model, the velocity u_α is updated only. It can be computed by considering the forcing term ψ_i as

$$u_\alpha = \sum_i c_{i\alpha} f_i + \frac{\delta_t}{2}\sum_i c_{i\alpha}\psi_i. \tag{34}$$

In addition, a correction term $s_i = -\frac{w_i}{2c_s^4}\mathscr{H}_{i,\alpha\beta}\nabla\Phi_{\alpha\beta\gamma}$ is added into forcing term to cancel symmetry-breaking errors $\Phi_{\alpha\beta\gamma}$, which is due to the topology of the nearest-neighbor lattice.[24,60] $\Phi_{\alpha\beta\gamma} = 0$ except for $\Phi_{\alpha\alpha\alpha}^{(3)} = -u_\alpha^3$, (here, α is related to components of Cartesian coordinates without summation over repeated index).

D. Finite volume method for scalar transport

In this paper, the continuity equation and momentum equation are solved by the lattice Boltzmann equation, while scalar transport equation is solved separately by finite type technique. Numerically, double distribution function models are not optimal from the computational standpoint despite there is no need to use a full set of distribution functions to simulate a scalar, even though this numerical inefficiency can be improved somewhat by using some redundant degree of freedom in LB models in diffusion dominated condition.[61] Considering that mass conservation, the energy (potential temperature) or scalar conservation equations can be expressed by following general convection-diffusion form:[48,62]

$$\frac{\partial \phi}{\partial t} + \boldsymbol{u}\cdot\nabla\phi = \nabla(\Gamma\nabla\phi) + Q_\phi, \tag{35}$$

where $\boldsymbol{u}$ is macroscopic velocity vector, ϕ is general scalar, and Γ is general diffusion coefficient. Q_ϕ is general source term which could represent Q_r in Eq. (6c). The explicit second-order Runge–Kutta scheme is adopted as temporal discretization, which is given as

$$\begin{aligned}\phi^{n+1/2} &= \phi^n + \frac{\delta t}{2}\left[F_C(\phi^n) + F_D(\phi^n) + Q_\phi^n\right]\\ \phi^{n+1} &= \phi^n + \delta t\left[F_C(\phi^{n+1/2}) + F_D(\phi^{n+1/2}) + Q_\phi^{n+1/2}\right],\end{aligned} \tag{36}$$

where F_C, F_D represents convection term and diffusion term. The general scalar conservation equation is spatially discretized using monotonic upwind scheme for conservation laws (MUSCL) and central difference (CD) schemes, where the MUSCL scheme is adopted for the convection term and the CD scheme for the diffusion term. The third-order MUSCL scheme[63] with the van Albada limiter function $\psi(r) = 2r/(1 + r^2)$ is adopted in this study and is used to avoid spurious oscillations. In the following study, ϕ represents potential temperature θ and convection-diffusion of potential temperature is solved by the finite volume method (FVM), which is an alternative formulation of energy equation and no heating rate is considered with $Q_\phi = 0$.

IV. NUMERICAL TESTS AND DISCUSSIONS

In order to assess the validity of the proposed regularized LB model for solving anelastic Eq. (10), atmospheric deep convection of thermal rising bubble, density currents in neutral atmospheric condition and inertia-gravity waves are analyzed and discussed in this section. The typical D2Q9 lattice stencil is employed in the simulations. The inviscid flows are treated as quasi-inviscid, with a very small non-dimensional viscosity $\nu = 10^{-15}$. The computational domain, boundary condition (BC), and initial perturbation in the three benchmarking test cases are summarized as follows:

(A) Atmospheric deep convection[64–67]
Domain: height of [0, 10] km and width of [0, 20 km].
Boundary: rigid wall BC on four sides.
Perturbation: $\theta' = 2\cos^2\frac{\pi L}{2}$, with $L = \sqrt{\frac{(x-x_c)^2}{x_r^2} + \frac{(z-z_c)^2}{z_r^2}}$, $x_c = 10.0$ km, $z_c = 2.0$ km, and $x_r = z_r = 2.0$ km.

(B) Density currents[68–70]

Domain: height of [0, 6.4] km and width of [−25.6, 25.6] km.
Boundary: rigid wall BC on top and bottom, periodic BC on lateral side.
Perturbation: $\theta' = -15\frac{1+\cos(\pi L)}{2}$, with $L = \sqrt{\frac{(x-x_c)^2}{x_r^2} + \frac{(z-z_c)^2}{z_r^2}}$, $x_c = 0.0$ km, $z_c = 3.0$ km, and $x_r = 4.0$ km, $z_r = 2.0$ km.

(C) Non-hydrostatic inertia-gravity waves[64,66,67]
Domain: height of [0, 10] km and width of [0, 300] km.
Boundary: rigid wall BC on top and bottom, periodic BC on lateral side.
Perturbation: $\theta' = 0.01\frac{\sin(\pi z/H)}{1+L^2}$, with $L = \frac{(x-x_c)}{x_r}$, $x_c = 100$ km and $x_r = 5$ km.

A. Atmospheric deep convection

A rising thermal bubble in deep atmosphere is examined using the present anelastic model. The simulation is two-dimensional, with a domain height of 10 km and width of 20 km.[64] Rigid wall boundary conditions are specified on all four sides of the domain. The initial unperturbed environment is calm (zero initial wind everywhere), hydrostatic, and neutrally stable, defined by a constant potential temperature of 300 K. The value of base state pressure at the surface p_{00} is 1000 mb, and the profile of base state fields is obtained by integrating the hydrostatic equation upwards with $\theta_s = 300$ K and gravity $g = 9.81$ m^2/s. A warm perturbation is placed at the center of the domain, which is specified by[65]

$$\theta' = 2\cos^2\frac{\pi L}{2}, \tag{37}$$

where

$$L = \sqrt{\frac{(x-x_c)^2}{x_r^2} + \frac{(z-z_c)^2}{z_r^2}}, \tag{38}$$

$x_c = 10.0$ km, $z_c = 2.0$ km, and $x_r = z_r = 2.0$ km. No physical or computational diffusion is applied as the simulation presented in Ref. 65, which is implemented by $\bar{\tau} \approx 0.5$ and $\nu = 0$ m^2/s in our simulation.

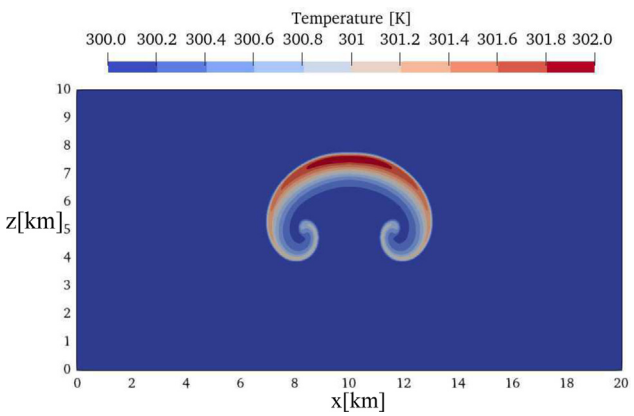

FIG. 1. Potential temperature at $t = 1000$ s obtained by the present anelastic LB model in simulation of rising thermal bubble. The unit of space of domain is km. Results are obtained on grid size $\delta x = 25$ m with parameters: viscosity $\nu = 0$ m^2/s, relaxation time $\bar{\tau} \approx 0.5$ and heat conductivity $\lambda = 0$ W/(m^2 K).

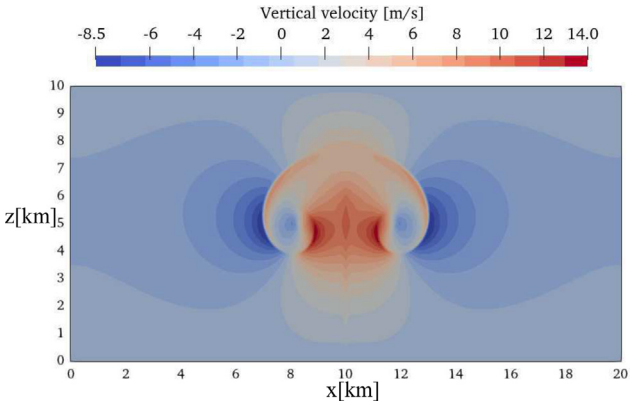

FIG. 2. Vertical velocity at $t = 1000$ s obtained by the present anelastic LB model in simulation of rising thermal bubble. The unit of space of domain is km. Results are obtained on grid size $\delta x = 25$ m with parameters: viscosity $\nu = 0$ m^2/s, relaxation time $\bar{\tau} \approx 0.5$ and heat conductivity $\lambda = 0$ W/(m^2 K).

Driven by buoyancy, the warm bubble rises and rolls up on the sides. The dynamics of the thermal rising bubble is reproduced by the anelastic LB model and unphysical wiggles are suppressed by regularization and MUSCL scheme. Results of a simulation with 25-m grid spacing after 1000 s of integration are presented in Figs. 1 and 2. In agreement with the results in Refs. 65 and 66, the warm bubble rises and expands over time. Two rotors develop on the sides of the warm bubble, while the top of the thermal is stretched. The benchmark solution in Ref. 65 was obtained with third-order Runge–Kutta time marching and fifth-order spatial derivatives on 100-m grid spacing.

Figures 1 and 2 display the temperature and vertical velocity contours obtained by anelastic LB model, respectively. It is seen that both the temperature field and velocity field obtained by the anelastic LBM model are in good agreement with results displayed in Refs. 65 and 66.

In order to quantitatively validate the proposed model, the values of the thermal perturbation amplitude are given in Table I. The computed final values of thermal perturbation are confirmed closely with benchmark solution in Ref. 65 and the soundproof results in the Ref. 67. The deviations increase when mesh size increased from 25 to 50 m. However, almost the same values of maxima and minima with compressible and soundproof results have been predicted by the proposed model in this test case. These values strongly suggest that the proposed model can give the same unsteady results with compressible and soundproof model, temporally and spatially. The simulations were carried on Dell workstation with 32 G RAM and 12 cores of

TABLE I. Comparison of maxima and minima of vertical velocity and perturbation potential temperature at final time $t = 1000$ s. Results are obtained by the present LB model with parameters: kinematic viscosity $\nu = 0$ m^2/s, relaxation time $\bar{\tau} = 0.5$ and heat conductivity $\lambda = 0$ W/(m^2 K) on spacing sizes 25 and 50 m.

	δx : 25 m	δx : 50 m	Reference 65	Reference 67
w_{max}	14.21	14.0	14.54	13.69
w_{min}	−8.68	−8.50	−8.58	−8.45
θ_{max}	1.96	1.90	2.07	1.54
θ_{min}	0.0	0.0	−0.14	−0.10

Xenon-6148 2.4 G Hz (OpenMPI used). The central processing unit (CPU) time for $\delta x = 25$ m and $\delta x = 50$ m is approximately 32 and 58 minutes, respectively.

B. Density currents under anelastic approximation

The second test consists of a negative potential temperature perturbation in a neutrally stratified atmosphere,[68,69]

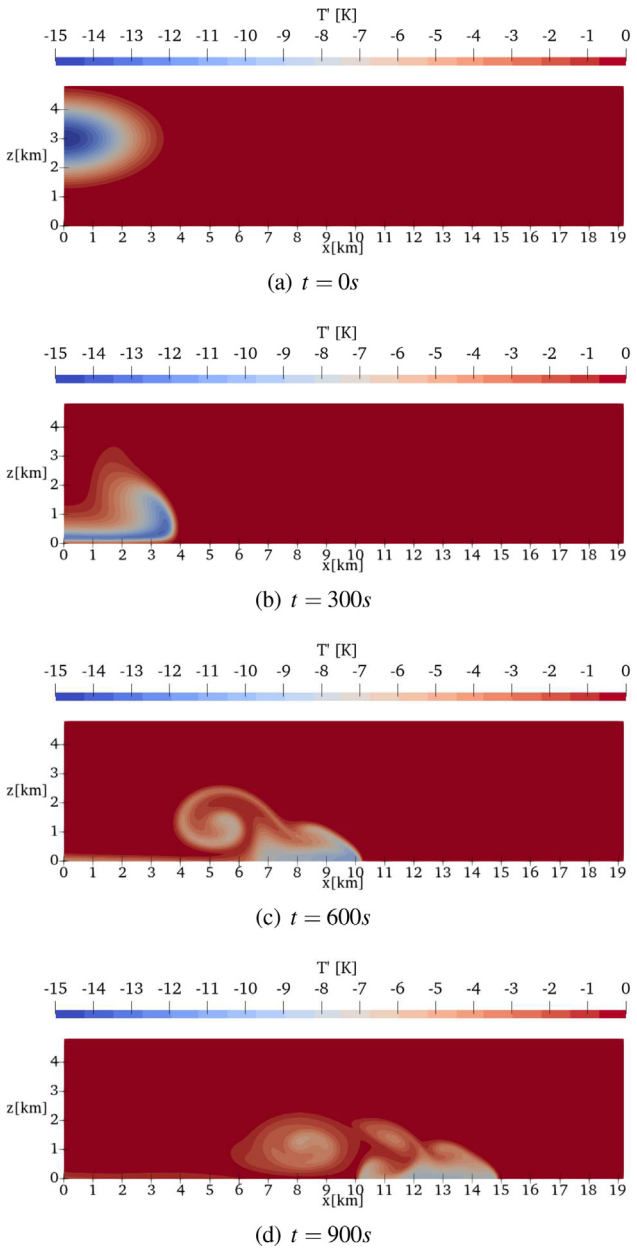

FIG. 3. Potential temperature perturbation obtained by anelastic LB model in the density currents test case. (a) $t = 0$ s, (b) $t = 300$ s, (c) $t = 600$ s, and (d) $t = 900$ s. The unit of domain axis is meter and potential temperature perturbation is in Kelvin. Results are obtained on grid size $\delta x = 25$ m with parameters: viscosity $\nu = 75.0$ m^2/s and diffusivity $\Gamma = 75.0$ m^2/s.

$$\theta' = -15\frac{1+\cos(\pi L)}{2}, \tag{39}$$

where

$$L = \sqrt{\frac{(x-x_c)^2}{x_r^2} + \frac{(z-z_c)^2}{z_r^2}}, \tag{40}$$

$x_c = 0.0$ km, $z_c = 3.0$ km, $x_r = 4.0$ km, and $z_r = 2.0$ km.

The simulation is also two-dimensional, with a domain height of [0, 6.4] km and width of [−25.6, 25.6] km. The boundary conditions are periodic on the left and right sides, solid walls on the top and bottom boundaries. The initial unperturbed environment is calm, hydrostatic, and neutrally stable, defined by a constant potential temperature $\theta_s = T_s$ of 300 K. The reference value of pressure p_{00} at the surface is 1000 mb. The profile of base state variables is calculated with θ_s and gravity $g = 9.81$ m^2/s. The initial velocity is set to zero in the whole domain.

Simulations based on the LB model with anelastic approximation are carried with $\delta x = 50$, 100, and 200 m. The selected kinematic viscosity and diffusivity are equal to $\nu = 75.0$ m^2/s and diffusivity $\Gamma = 75.0$ m^2/s, respectively. Initially, the negative buoyancy of the bubble drives it down, until it hits the bottom boundary and starts spreading in the horizontal direction with small-scale Kelvin–Helmholtz instabilities. Due to the symmetry of the test case, only the sub-domain [0, 19.2] km × [0, 4.8] km is shown in Fig. 3. The method recovers well the flow patterns at the different scales and gives a good representation of the vortices. The benchmark solution is given in Refs. 68 and 70 by high-order and spectral type schemes on 100-m resolution.

Comparison of front location at 900 s obtained by the proposed model and results in literature[68,70] is reported in Table II. The value of location is in good agreement with reference values. It is shown that our anelastic LB model has obtained almost the same front location compared with results in Ref. 70 and results.[68] The differences increase when mesh size is increased from 50 to 200 m. However, the maximum deviation remains within 1%.

C. Non-hydrostatic inertia-gravity waves

The last test case deals with a perturbation on the thermally stratified background with a horizontal flow $u = 20$ m · s^{-1}.[64,67] Different with previous two test cases, a stratification effect is introduced by the Brunt–Väisälä frequency,

$$N = \sqrt{\frac{g}{\theta_s}\frac{\mathrm{D}\theta_s}{\mathrm{D}z}}. \tag{41}$$

TABLE II. Comparison of front location at 900 s. In data listed in Ref. 68, AFD represents the results by a quasi-compressible high-order finite difference method, MUa is the result given by an anelastic solver and REFQ presents the results obtained by the other quasi-compressible solver.

δx	Present	Bryan[70]	Straka *et al.*[68]
50 m	15.37 km	15.375 km	AFD: 15.17 km
100 m	14.9 km	15.45 km	MUa: 14.56 km
200 m	14.4 km	15.50 km	REFQ: 15.51 km

In this case, we obtain the range θ_s [300, 332.19] K for z [0, 10] km in the background thermal stratification with the values $N = 0.01$ s^{-1}, $g = 9.81$ m $\cdot$ s^{-2}, and $\theta_{s,0} = 300$ K. In a [0, 300] $\times$ [0, 10] km^2 domain, the following initial perturbation is introduced:

$$\theta' = 0.01 \frac{\sin(\pi z/H)}{1 + L^2}, \tag{42}$$

where

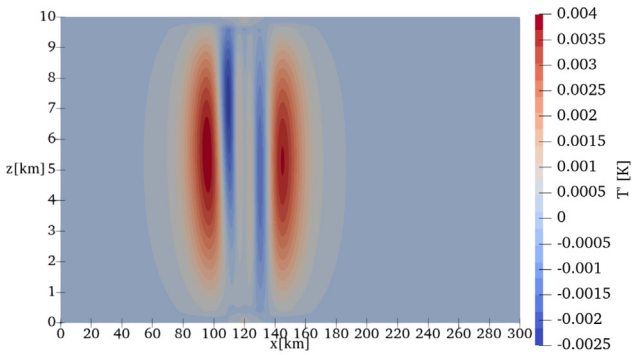

(a) $t = 1000s$

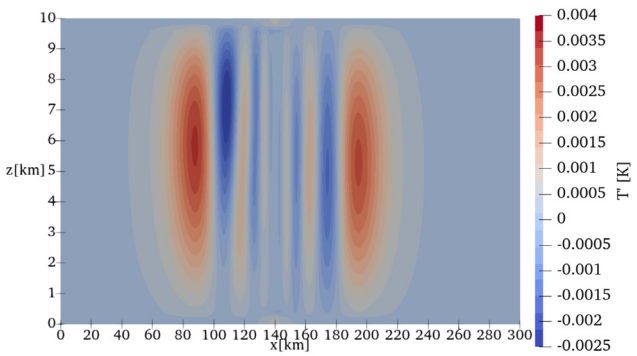

(b) $t = 2000s$

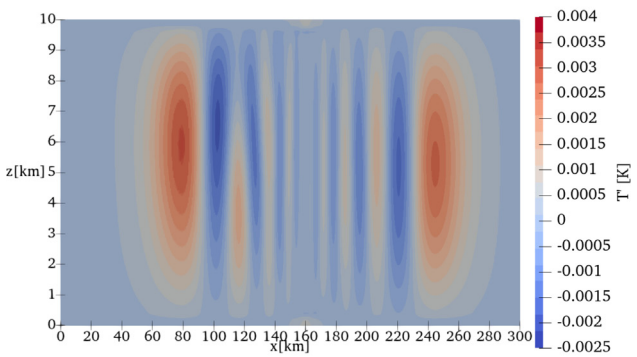

(c) $t = 3000s$

FIG. 4. Potential temperature perturbation in non-hydrostatic inertia-gravity waves. (a) $t = 1000$ s, (b) $t = 2000$ s, and (c) $t = 3000$ s. Computed solution by the anelastic LB model with $\delta x = 400$ m.

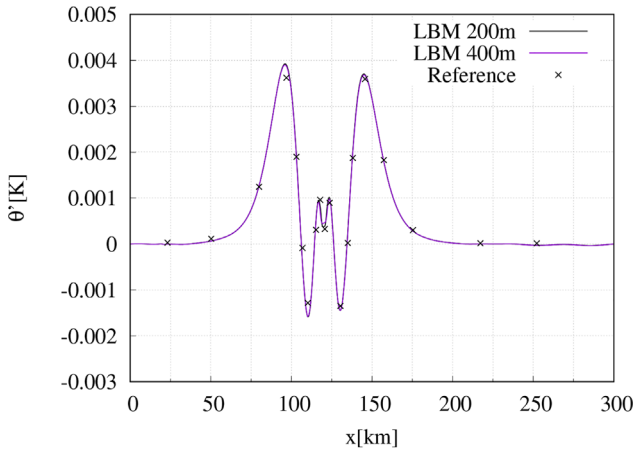

(a) $t = 1000s$

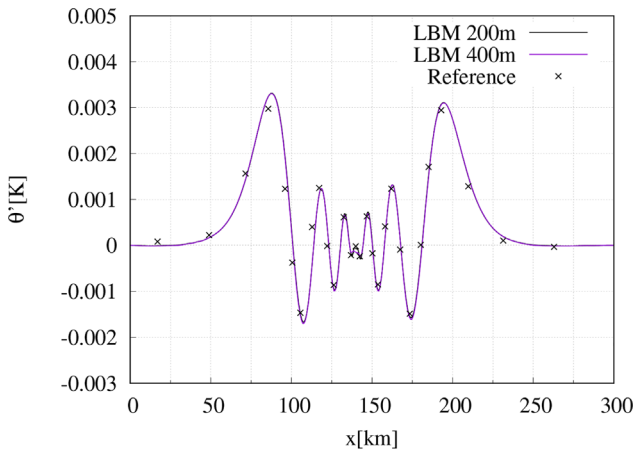

(b) $t = 2000s$

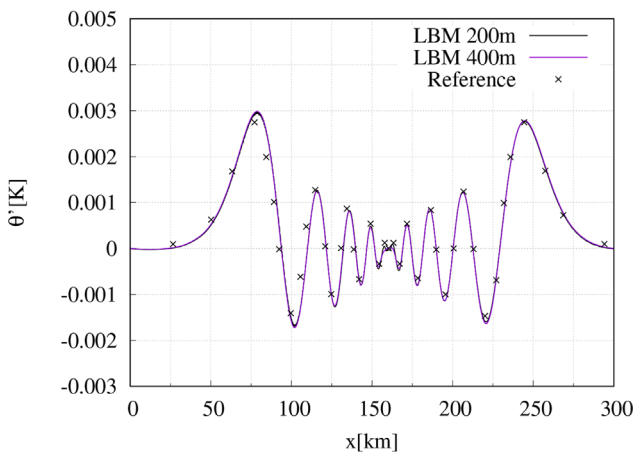

(c) $t = 3000s$

FIG. 5. Potential temperature perturbation compared with reference solution.[67] (a) $t = 1000$ s, (b) $t = 2000$ s, and (c) $t = 3000$ s. Our results are computed solution by the anelastic LB model with $\delta x = 400$ m and $\delta x = 200$ m, non-dimensional relaxation time is close to $\bar{\tau} = 0.5$. The reference results (cross) were obtained by a blended soundproof-to-compressible numerical model.

$$L = \frac{(x - x_c)}{x_r}, \tag{43}$$

$x_c = 100.0$ km, $H = 10.0$ km, and $x_r = 5.0$ km. With the same treatment as in the previous cases, boundary conditions are set periodic on the lateral sides while solid walls conditions are imposed on top and bottom boundaries. Unlike the previous test cases, here the dominant physical mechanism is chiefly wavelike rather than vertically buoyancy-driven. Inertia-gravity waves develop in the horizontal direction. The simulation is performed with $\delta x = 200$ and 400 m, corresponding time step approximately equals to 0.4, 0.8 s, respectively. The kinematic viscosity $\nu = 10.0$ m^2/s and diffusivity $\Gamma = 10.0$ m^2/s are adopted in the simulation.

In order to compare the present results with the benchmark solutions given in the literature,[66,67] the present results of wave pattern of the potential temperature field are shown in Fig. 4. It can be observed from Fig. 4 that the present results obtained by the LB method with anelastic model agree well with the results in literature.

A quantitative comparison between the results obtained by the present model and the results in Ref. 67 is reported in Fig. 5. The solution in Ref. 67 was obtained using a blended soundproof-to-compressible numerical model with the second-order finite volume discretization. Potential temperature perturbations through horizontal centerline using a horizontal cuts of the two-dimensional plots at height $z = 5000$ m are shown in those figures. Moreover, the potential temperature profile at time $t = 1000$, 2000, and 3000 s are in very good agreement with the data in literature. The maxima and minima of perturbations of potential temperature are in line with published works. The present results show that the anelastic LB model with the regularized scheme and hybrid thermal model can be applied for non-hydrostatic inertia-gravity waves problems, and the well performances of the present method for this kind of atmospheric problems are demonstrated.

V. CONCLUSIONS

In this paper, an LB-based anelastic model for atmospheric convection is proposed. A regularized BGK model is employed in LB equation and finite volume scheme is adopted on energy-conservation equation. Based on the standard LB model for flows at nearly constant density, the external force terms are derived to incorporate non-hydrodynamic modes under anelastic approximation. The macroscopic governing equations and effects of force terms under anelastic and Boussinesq approximations are analyzed and discussed by Chapman–Enskog asymptotic expansion. Three benchmark problems have been used to assess the new model: a non-hydrostatic atmospheric convection, two-dimensional density currents, and inertia-gravity waves in stable atmospheric layer have been investigated. The validations demonstrate that the present extension of the LBM can simulate atmospheric flows under anelastic approximation accurately.

ACKNOWLEDGMENTS

This work was supported by ANR Industrial Chair ALBUMS (Grant No. ANR-18-CHIN-0003-01). This work was performed using HPC resources from GENCI-TGCC/CINES (Grant No. 2018-A0032A07679).

DATA AVAILABILITY

The data that support the findings of this study are available from the corresponding author upon reasonable request.

REFERENCES

[1]B. Blocken, "Computational fluid dynamics for urban physics: Importance, scales, possibilities, limitations and ten tips and tricks towards accurate and reliable simulations," Build. Environ. **91**, 219–245 (2015).
[2]D. Muñoz-Esparza, B. Kosović, J. Van Beeck, and J. Mirocha, "A stochastic perturbation method to generate inflow turbulence in large-eddy simulation models: Application to neutrally stratified atmospheric boundary layers," Phys. Fluids **27**, 035102 (2015).
[3]S. Xie, D. Yang, Y. Liu, and L. Shen, "Simulation-based study of wind loads on semi-submersed object in ocean wave field," Phys. Fluids **28**, 015106 (2016).
[4]R. Klein, "Asymptotics, structure, and integration of sound-proof atmospheric flow equations," Theor. Comput. Fluid Dyn. **23**, 161–195 (2009).
[5]P. R. Bannon, "On the anelastic approximation for a compressible atmosphere," J. Atmos. Sci. **53**, 3618–3628 (1996).
[6]W. W. Grabowski and P. K. Smolarkiewicz, "A multiscale anelastic model for meteorological research," Mon. Weather Rev. **130**, 939–956 (2002).
[7]L. K. Currie and S. M. Tobias, "Mean flow generation in rotating anelastic two-dimensional convection," Phys. Fluids **28**, 017101 (2016).
[8]C. Gatti-Bono and P. Colella, "An anelastic allspeed projection method for gravitationally stratified flows," J. Comput. Phys. **216**, 589–615 (2006).
[9]A. Inagaki, M. Kanda, N. H. Ahmad, A. Yagi, N. Onodera, and T. Aoki, "A numerical study of turbulence statistics and the structure of a spatially-developing boundary layer over a realistic urban geometry," Boundary-Layer Meteorol. **164**, 161–181 (2017).
[10]S. Lenz, M. Schoenherr, M. Geier, M. Krafczyk, A. Pasquali, A. Christen, and M. Giometto, "Towards real-time simulation of turbulent air flow over a resolved urban canopy using the cumulant lattice Boltzmann method on a GPGPU," J. Wind Eng. Ind. Aerodyn. **189**, 151–162 (2019).
[11]Y. Feng, P. Boivin, J. Jacob, and P. Sagaut, "Hybrid recursive regularized lattice boltzmann simulation of humid air with application to meteorological flows," Phys. Rev. E **100**, 023304 (2019).
[12]Y. Feng, J. Miranda-Fuentes, S. Guo, J. Jacob, and P. Sagaut, "ProLB: A lattice Boltzmann solver of large-eddy simulation for atmospheric boundary layer flows," J. Adv. Model. Earth Syst. **13**, e2020MS002107 (2021).
[13]S. Succi, *The Lattice Boltzmann Equation: For Fluid Dynamics and Beyond*, Numerical Mathematics and Scientific Computation (Clarendon Press, 2001).
[14]A. A. Mohamad, *Lattice Boltzmann Method: Fundamentals and Engineering Applications with Computer Codes* (Springer-Verlag, London, 2001).
[15]J. Jacob and P. Sagaut, "Wind comfort assessment by means of large eddy simulation with lattice Boltzmann method in full scale city area," Build. Environ. **139**, 110–124 (2018).
[16]S. Wilhelm, J. Jacob, and P. Sagaut, "A new explicit algebraic wall model for LES of turbulent flows under adverse pressure gradient," Flow, Turbul. Combust. **106**, 1–35 (2021).
[17]P. Lallemand and L. S. Luo, "Hybrid finite-difference thermal lattice Boltzmann equation," Int. J. Mod. Phys. B **17**, 41–47 (2003).
[18]Z. Chen, C. Shu, L. Yang, X. Zhao, and N. Liu, "Immersed boundary–simplified thermal lattice Boltzmann method for incompressible thermal flows," Phys. Fluids **32**, 013605 (2020).
[19]D. Wang, D. Tan, and N. Phan-Thien, "A lattice Boltzmann method for simulating viscoelastic drops," Phys. Fluids **31**, 073101 (2019).
[20]X. Li, Z.-Q. Dong, P. Yu, X.-D. Niu, L.-P. Wang, D.-C. Li, and H. Yamaguchi, "Numerical investigation of magnetic multiphase flows by the fractional-step-based multiphase lattice Boltzmann method," Phys. Fluids **32**, 083309 (2020).
[21]B. J. Palmer and D. R. Rector, "Lattice Boltzmann algorithm for simulating thermal flow in compressible fluids," J. Comput. Phys. **161**, 1–20 (2000).
[22]Q. Li, K. Luo, Y. He, and W. Tao, "Coupling lattice Boltzmann model for simulation of thermal flows on standard lattices," Phys. Rev. E **85**, 016710 (2012).
[23]M. H. Saadat, F. Bösch, and I. V. Karlin, "Lattice Boltzmann model for compressible flows on standard lattices: Variable Prandtl number and adiabatic exponent," Phys. Rev. E **99**, 013306 (2019).

[24]Y. Feng, P. Boivin, J. Jacob, and P. Sagaut, "Hybrid recursive regularized thermal lattice Boltzmann model for high subsonic compressible flows," J. Comput. Phys. **394**, 82–99 (2019).
[25]Q. Zou, S. Hou, S. Chen, and G. D. Doolen, "A improved incompressible lattice Boltzmann model for time-independent flows," J. Stat. Phys. **81**, 35–48 (1995).
[26]X. Y. He, S. Y. Chen, and G. D. Doolen, "A novel thermal model for the lattice Boltzmann method in incompressible limit," J. Comput. Phys. **146**, 282–300 (1998).
[27]Z. Guo, B. Shi, and N. Wang, "Lattice BGK model for incompressible Navier-Stokes equation," J. Comput. Phys. **165**, 288–306 (2000).
[28]P. J. Dellar, "Nonhydrodynamic modes and a priori construction of shallow water lattice Boltzmann equations," Phys. Rev. E **65**, 036309 (2002).
[29]J. Zhou, "A lattice Boltzmann model for the shallow water equations," Comput. Methods Appl. Mech. Eng. **191**, 3527–3539 (2002).
[30]Z. Linhao, F. Shide, and G. Shouting, "Wind-driven ocean circulation in shallow water lattice Boltzmann model," Adv. Atmos. Sci. **22**, 349–358 (2005).
[31]S. Venturi, S. D. Francesco, M. Geier, and P. Manciola, "A new collision operator for lattice Boltzmann shallow water model: A convergence and stability study," Adv. Water Resour. **135**, 103474 (2020).
[32]P. L. Bhatnagar, E. P. Gross, and M. Krook, "A model for collision processes in gases. I. small amplitude processes in charged and neutral one-component systems," Phys. Rev. **94**, 511–525 (1954).
[33]P. Lallemand and L. S. Luo, "Theory of the lattice Boltzmann method: Acoustic and thermal properties in two and three dimensions," Phys. Rev. E **68**, 036706 (2003).
[34]N. I. Prasianakis, S. S. Chikatamarla, I. V. Karlin, S. Ansumali, and K. Boulouchos, "Entropic lattice boltzmann method for simulation of thermal flows," Math. Comput. Simul. **72**, 179–183 (2006).
[35]M. Geier, A. Greiner, and J. G. Korvink, "Cascaded digital lattice Boltzmann automata for high reynolds number flow," Phys. Rev. E **73**, 066705 (2006).
[36]M. Geier, A. Greiner, and J. Korvink, "A factorized central moment lattice Boltzmann method," Eur. Phys. J.-Spec. Top. **171**, 55–61 (2009).
[37]X. Shan, "Central-moment-based Galilean-invariant multiple-relaxation-time collision model," Phys. Rev. E **100**, 043308 (2019).
[38]M. Geier, M. Schönherr, A. Pasquali, and M. Krafczyk, "The cumulant lattice boltzmann equation in three dimensions: Theory and validation," Comput. Math. Appl. **70**, 507–547 (2015).
[39]J. Latt and B. Chopard, "Lattice Boltzmann method with regularized pre-collision distribution functions," Math. Comput. Simul. **72**, 165–168 (2006).
[40]K. K. Mattila, P. C. Philippi, and L. A. Hegele, Jr., "High-order regularization in lattice-Boltzmann equations," Phys. Fluids **29**, 046103 (2017).
[41]C. Coreixas, G. Wissocq, G. Puigt, J. Boussuge, and P. Sagaut, "Recursive regularization step for high-order lattice Boltzmann methods," Phys. Rev. E **96**, 033306 (2017).
[42]A. Mezrhab, M. Bouzidi, and P. Lallemand, "Hybrid lattice-Boltzmann finite-difference simulation of convective flows," Comput. Fluids **33**, 623–641 (2004).
[43]J. Tölke, "A thermal model based on the lattice Boltzmann method for low Mach number compressible flows," J. Comput. Theor. Nanosci. **3**, 579–587 (2006).
[44]Q. Li and K. H. Luo, "Effect of the forcing term in the pseudopotential lattice Boltzmann modeling of thermal flows," Phys. Rev. E **89**, 053022 (2014).
[45]Y.-L. Feng, S.-L. Guo, W.-Q. Tao, and P. Sagaut, "Regularized thermal lattice Boltzmann method for natural convection with large temperature differences," Int. J. Heat Mass Transfer **125**, 1379–1391 (2018).
[46]M. Duarte, A. S. Almgren, and J. B. Bell, "A low Mach number model for moist atmospheric flows," J. Atmos. Sci. **72**, 1605–1620 (2015).
[47]D. J. Raymond, "Sources and sinks of entropy in the atmosphere," J. Adv. Modeling Earth Syst. **5**, 755–763 (2013).
[48]F. White, *Fluid Mechanics*, McGraw-Hill Series in Mechanical Engineering (McGraw Hill, 2011).
[49]Y. Ogura and N. A. Phillips, "Scale analysis of deep and shallow convection in the atmosphere," J. Atmos. Sci. **19**, 173–179 (1962).
[50]R. Klein and A. J. Majda, "Systematic multiscale models for deep convection on mesoscales," Theor. Comput. Fluid Dyn. **20**, 525–551 (2006).
[51]D. Lilly, "A comparison of incompressible, anelastic and Boussinesq dynamics," Atmos. Res. **40**, 143–151 (1996).
[52]B. Stevens, C.-H. Moeng, A. S. Ackerman, C. S. Bretherton, A. Chlond, S. de Roode, J. Edwards, J.-C. Golaz, H. Jiang, M. Khairoutdinov, M. P. Kirkpatrick, D. C. Lewellen, A. Lock, F. Müller, D. E. Stevens, E. Whelan, and P. Zhu, "Evaluation of large-Eddy simulations via observations of nocturnal marine stratocumulus," Mon. Weather Rev. **133**, 1443–1462 (2005).
[53]Y. Qian, D. D'HumiÃres, and P. Lallemand, "Lattice BGK models for Navier-Stokes equation," Europhys. Lett. **17**, 479–484 (1992).
[54]S. Y. Chen and G. D. Doolen, "Lattice Boltzmann method for fluid flows," Annu. Rev. Fluid Mech. **30**, 329–364 (1998).
[55]P. J. Dellar, "An interpretation and derivation of the lattice Boltzmann method using strang splitting," Comput. Math. Appl. **65**, 129–141 (2013).
[56]X. W. Shan, X. F. Yuan, and H. D. Chen, "Kinetic theory representation of hydrodynamics: A way beyond the Navier-Stokes equation," J. Fluid Mech. **550**, 413–441 (2006).
[57]R. Zhang, X. Shan, and H. Chen, "Efficient kinetic method for fluid simulation beyond the Navier-Stokes equation," Phys. Rev. E **74**, 046703 (2006).
[58]C. Zhuo and P. Sagaut, "Acoustic multipole sources for the regularized lattice Boltzmann method: Comparison with multiple-relaxation-time models in the inviscid limit," Phys. Rev. E **95**, 063301 (2017).
[59]J. Jacob, O. Malaspinas, and P. Sagaut, "A new hybrid recursive regularised Bhatnagar–Gross–Krook collision model for lattice Boltzmann method-based large eddy simulation," J. Turbul. **19**, 1051–1076 (2018).
[60]S. Guo, Y. Feng, J. Jacob, F. Renard, and P. Sagaut, "An efficient lattice Boltzmann method for compressible aerodynamics on D3Q19 lattice," J. Comput. Phys. **418**, 109570 (2020).
[61]L. Li, R. Mei, and J. F. Klausner, "Lattice Boltzmann models for the convection-diffusion equation: D2Q5 vs D2Q9," Int. J. Heat Mass Transfer **108**, 41–62 (2017).
[62]T. Stocker, *Introduction to Climate Modelling*, Advances in Geophysical and Environmental Mechanics and Mathematics (Springer, Berlin/Heidelberg, 2011).
[63]K. H. Kim, C. Kim, and O.-H. Rho, "Methods for the accurate computations of hypersonic flows: I. AUSMPW+ scheme," J. Comput. Phys. **174**, 38–80 (2001).
[64]L. J. Wicker and W. C. Skamarock, "A time-splitting scheme for the elastic equations incorporating second-order Runge–Kutta time differencing," Mon. Weather Rev. **126**, 1992–1999 (1998).
[65]G. H. Bryan and J. M. Fritsch, "A benchmark simulation for moist nonhydrostatic numerical models," Mon. Weather Rev. **130**, 2917–2928 (2002).
[66]T. Benacchio, W. P. O'Neill, and R. Klein, "A blended soundproof-to-compressible numerical model for small- to mesoscale atmospheric dynamics," Mon. Weather Rev. **142**, 4416–4438 (2014).
[67]T. Benacchio, "A blended semi-implicit numerical model for weakly compressible atmospheric dynamics," Ph.D. thesis (Freie Universität, Berlin, 2014).
[68]J. M. Straka, R. B. Wilhelmson, L. J. Wicker, J. R. Anderson, and K. K. Droegemeier, "Numerical solutions of a non-linear density current: A benchmark solution and comparisons," Int. J. Numer. Methods Fluids **17**, 1–22 (1993).
[69]L. J. Wicker and W. C. Skamarock, "Time-splitting methods for elastic models using forward time schemes," Mon. Weather Rev. **130**, 2088–2097 (2002).
[70]See http://www2.mmm.ucar.edu/people/bryan/cm1/test_gravity_current/ for "G. H. Bryan's cm1 test about gravity current" (2020).